JJEE
Volume X | Number X | Month 20XX | Pages XXX-XXX

Jordan Journal of Electrical Engineering

ISSN (print): 2409-9600, ISSN (online): 2409-9619

Homepage: jjee.ttu.edu.jo

A Compact and Flexible Rectenna for 915 MHz Wireless Radio Frequency Energy Harvesting

Saif M. Almadamegha[1], Rula S. Alrawashdeh[*2], Saqer S. Alja'aferh[3]

[1, 2, 3] Electrical Engineering Department, College of Engineering, Mutah University, Al-Karak, Jordan
E-mail: rular18@mutah.edu.jo

Received: Oct 15, 2024 *Revised: Jan 10, 2025* *Accepted: Jan 18, 2025* *Available online: Feb 18, 2025*

***Abstract*—** In this paper, a radio frequency energy harvesting rectenna system operating in the 915 MHz industrial scientific medical (ISM) band is designed and proposed. The proposed design - which consists of a flexible loop antenna, rectifier and matching section - has a small overall footprint area of 50×50 mm^2 ($0.15\lambda_0 \times 0.15\lambda_0$) and achieves a power conversion efficiency of up to 80% for an input power of 5 dBm and load resistance of 20 kΩ. The system also demonstrates efficient performance, obtaining a high-power conversion efficiency of about 58% for a small input power of -15 dBm which represents an actual case of a small power captured from ambient resources. This is considered as the highest reported power conversion efficiency for a flexible energy harvesting system at 915 MHz with such a small size and an input power level of only -15 dBm. The proposed rectenna system has many appealing features, small size, flexibility, and relatively high-power conversion efficiency which make it a good candidate for energy harvesting applications.

***Keywords*—** Energy harvesting; Industrial Scientific Medical band; Flexible rectenna; Loop antenna.

1. INTRODUCTION

Radio frequency energy harvesting (RFEH) is a "green or renewable" self-sustaining process of providing an endless source of energy from the available Electromagnetic (EM) fields that exist in the environment. The harvested-energy can be utilized for different applications, such as powering low-power devices in sensor networks and IoT applications [1]. This helps in reducing the needs for batteries, which not only add to the device's cost, weight, and size but also makes battery replacement expensive and time-consuming.

A typical RFEH system is shown in Fig. 1. Such a system is composed of: i) an antenna to capture the radio frequency (RF) energy, ii) an RF-DC converter, which converts the received high-frequency alternating current (AC) signal into a direct current (DC) power delivered to the load and iii) a matching circuit which passes the largest of the input power from the antenna to the rectifier [2-3]. In such a system, the antenna is required to: i) be small in size to fit in modern devices, ii) have a large gain to increase the effective area of capturing EM waves and iii) have an omnidirectional radiation pattern to harvest energy from different directions. The antenna is also preferred to be flexible in order to evacuate larger internal space of the device and lighten the overall device weight [4-5].

The rectifier is also required to exhibit a high RF-to-DC conversion efficiency. It is also important to match the antenna to the rectifier to reduce power reflections in between.

Meeting all these requirements simultaneously presents several challenges that earlier designs sought to address. However, these designs were either large in size [6-9], rigid [10-14],

* Corresponding author
DOI: https://doi.org/ 10.5455/jjee.204-1729017064

or had relatively low power conversion efficiency [15-18]. Different frequency bands have been exploited in previous work for different applications, scientific, and medical (ISM) band for powering implantable devices [19], 902-925 MHz for passive radio frequency identification (RFID) systems [20], 1800 MHz for global system for mobile communication (GSM) energy harvesting [21], and the 2.4-2.5 GHz ISM band for energy harvesting from wireless fidelity (WiFi) [8, 16, 21, 22]. Higher frequency bands for energy harvesting offer the potential for greater energy capture due to the higher energy density available at these frequencies [23].

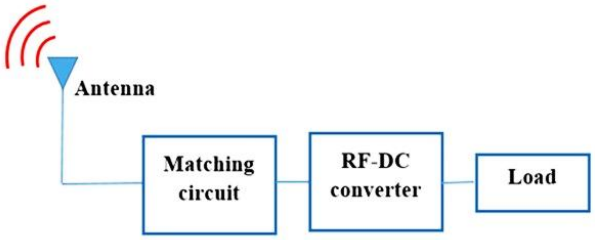

Fig. 1. A typical RFEH system.

Energy harvesting from higher frequency bands (above 1 GHz) is associated with larger RF energy availability from modern wireless communication systems, including Wi-Fi (2.4 GHz and 5 GHz) and 5G (sub-6 GHz and millimeter waves) [16, 24]. These frequencies offer higher power densities, making them attractive for energy harvesting applications. However, despite the advantage of smaller antenna sizes at higher frequencies, there are greater attenuation losses. To avoid such losses, designing RFEH rectennas to harvest RF energy below 1 GHz (like 915 MHz mobile handset RFID applications) becomes more attractive [25], especially when the issue of large size is addressed by using small footprint antenna structures like shorted-loop antennas [26].

The rectifier plays a major role in the rectenna design, and different topologies can be utilized as a rectifier circuit. These include the single diode [7, 8, 12, 15, 16, 27], voltage-doubler [6, 13, 14, 18, 19, 28-30], voltage multiplier [31] rectifiers, and others [17]. While single diode rectifiers are simple, they suffer from low efficiency due to the significant forward voltage drop and less effective utilization of the AC waveform. The efficiency also tends to decrease for the Greinacher voltage multiplier as more stages are added, due to the increasing voltage drop across each diode and the cumulative effect of capacitor losses. The voltage doubler uses two diodes and capacitors to effectively double the output voltage compared to single-diode rectifiers while keeping the overall design relatively simple [28].

A crucial requirement of rectennas is good matching with the rectifier. Different types of matching circuits can be used. Both LC matching networks and transmission lines can be used for impedance matching in RF circuits. However, LC matching networks are often preferred over transmission lines at the 915 MHz band because they can be more compact and simpler in design and implementation [29].

To overcome previous shortcomings and satisfy the current needs of an efficient rectenna design at the 915 MHz band, a small flexible rectenna system in the 915 MHz ISM band is proposed in this paper. The proposed system has many appealing features, such as small size, flexibility and relatively large power conversion efficiency (PCE) of up to 80% making it a good candidate for the applications of energy harvesting.

This paper is organized as follows: In Section 2, the design of each of the antenna, matching circuit and rectifier is proposed. The performance of the overall rectenna system is

then evaluated and discussed with a state-of-the-art comparison in Section 3. The paper is finally concluded in the last section.

2. STRUCTURES AND DESIGN

As stated above, the proposed rectenna system is composed of three main components: the antenna, rectifier, and matching circuit in between. The design of each component is presented in this section.

2.1. Antenna Design Using CST Microwave Studio

The antenna of the rectenna system proposed in this paper is aimed to satisfy the following requirements:

a) Resonance in the 915 MHz ISM band.
b) A size of not larger than 50×50 mm^2. This size is targeted to be smaller than the smallest flexible rectenna design in the literature which was 92×76 mm^2 at 915 MHz.
c) Omnidirectional radiation pattern. This is preferred to harvest energy at different angles and from different directions.
d) Flexibility. This is desired for modern wireless devices that need to be small in size and lightweight. The flexible antenna is usually very thin, leavening more internal space in the device. This space can either be saved for a smaller overall size or exploited to use internal components other than the antenna, such as sensors, enabling the device to support further functionalities [32-34].
e) Good gain value. The input power received (P_{in} (W)) by the antenna at the rectenna front increases with the antenna gain value (G_r). The antenna tends to have a larger effective area when its gain increases.

$$P_{in} = (P_d)(A_{eff}) \tag{1}$$

$$= \left(\frac{P_t G_t}{4\pi r^2}\right)\left(\frac{\lambda^2 G_r}{4\pi}\right) \tag{2}$$

$$= \frac{P_t G_t G_r}{(4\pi r \setminus \lambda)^2} \tag{3}$$

where P_d (W/m^2) is the power density, A_{eff} (m^2) is the antenna effective area, P_t (W) is the transmitted power, G_t is the transmitter antenna gain, G_r is the receiver antenna gain, r (m) is the distance between the transmitting and receiving antennas and λ (m) is the free space wavelength.

When a large AC power is picked up by the antenna, a large DC power will be converted and transferred to the load.

One of the effective structures to satisfy the above-mentioned requirements with flexibility is the loop structure which is selected for the proposed design [35]. The antenna is designed using Computer Simulation Technology (CST) software [36]. The antenna underwent several optimization steps to achieve resonance in the 915 MHz band while simultaneously meeting other design objectives. The following summarizes the design steps:

- Step 1: the antenna structure in this step is shown in Fig. 2.

The antenna consists of two loops: an outer loop and an inner loop. The main outer loop is fed through inductive coupling, which is caused by an inner rectangular loop that is located inside the outer loop. The inner loop is fed directly through a 50 Ω port. A dielectric substrate made from polypropylene is used as a loading material with a relative dielectric constant of ε_r= 2.26, and a loss tangent about 0.00043 [37]. It is worth indicating that a flexible copper tape can be used for realization. Polypropylene was selected for its flexible material. Initially, the antenna resonated around 1400 MHz at this stage, which is still suboptimal, as shown in Fig. 3.

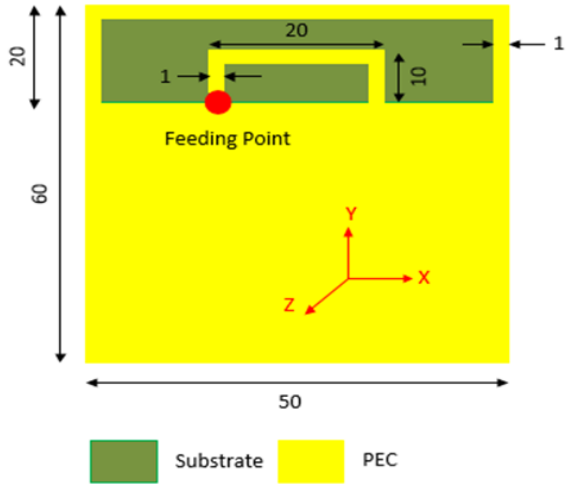

Fig. 2. Initial structure of the proposed antenna (dimensions in mm.)

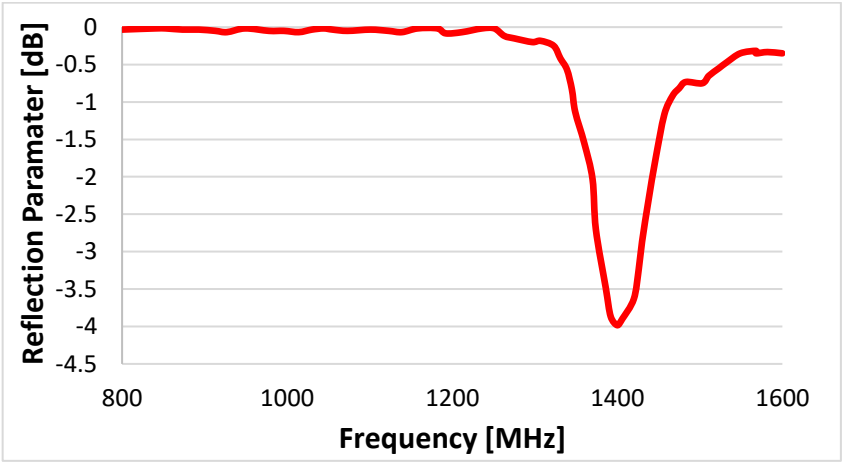

Fig. 3. Reflection coefficient S11 of the proposed antenna in step 1.

- Step 2: the antenna is miniaturized at this stage by meandering the outer loop.

The meandered loop increased the current path shifting the resonant frequency down to 1250 MHz with a size reduction to 50 × 40 mm². The antenna structure and reflection coefficient at this stage are shown in Figs. 4 and Fig. 5, respectively. Each pair of meandered segments resembles the plates of a parallel plate capacitor of which the capacitance C (F) is mainly affected by the spacing in between (d (m)) [38].

$$C = \frac{\varepsilon A}{d} \tag{4}$$

where ε (F/m) is the effective permittivity of the material between the conducting meandered parts and A (m²) is the area of the plate resembled by the meandered part.

The resonant frequency (f_r (Hz)) is controlled by C as [39]:

$$f_r = \frac{1}{\sqrt{LC}} \tag{5}$$

where L (H) is the effective inductance.

The radiation efficiency (η) is also noticed to increase by 20% at the resonant frequencies from step 1 to step 2. This can be attributed to the increased area of the radiating part of the outer loop, which results in a reduction of the overall resistance (R (Ω)) and consequently decreases the Ohmic losses dissipated in the loss resistance (Ω) accordingly [40].

$$R \propto \frac{1}{A} \tag{6}$$

$$\eta = \frac{R_r}{R_r + R_L} \tag{7}$$

where R_r (Ω) is the radiation resistance and R_L (Ω) is the loss resistance.

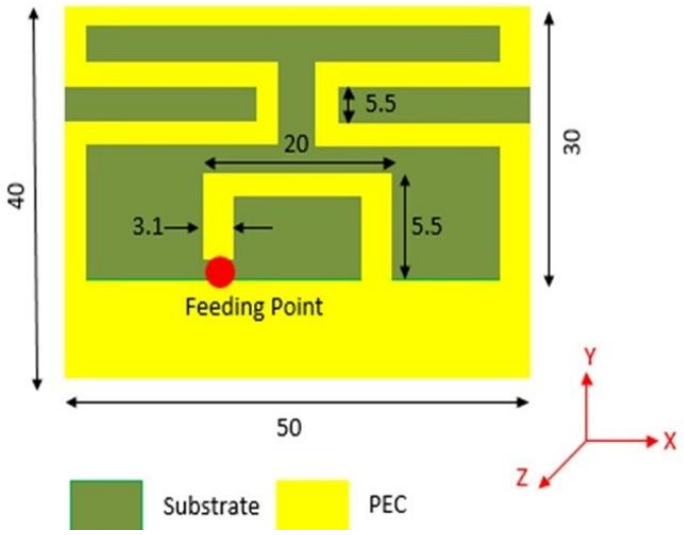

Fig. 4. The proposed antenna in stage 2 (dimensions in mm.)

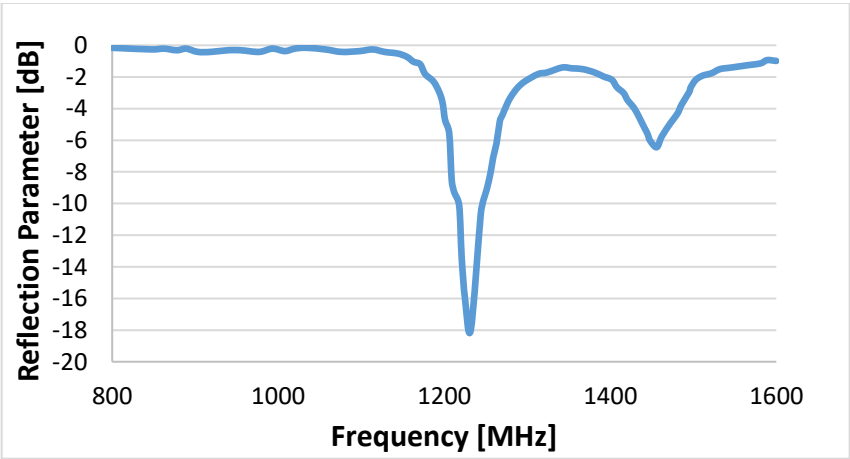

Fig. 5. Reflection coefficient S_{11} of the proposed antenna in step 2.

- Step 3: The antenna performance is optimized with a modified ground structure at this stage by applying two important techniques:

a) Reducing the width of the loop's strip: this increases the inductance of the design, further shifting the resonant frequency down towards the desired frequency band.
b) Defecting the ground: this technique increases the electrical length of the loop antennas (L-shaped slots are created near the lower corners of the proposed design), and tunes the level of matching by the capacitance introduced from the stepped-ground plane [41]. The proposed design is shown in Fig. 6. These two techniques lead to a miniaturized design operating with S11< -10 dB over the frequency band 905-925 MHz, as depicted from Fig. 7. This percentage bandwidth is 4.8% only which is considered narrow. However, it is wide enough to satisfy the intended applications over the frequency band of interest (902-925 MHz).

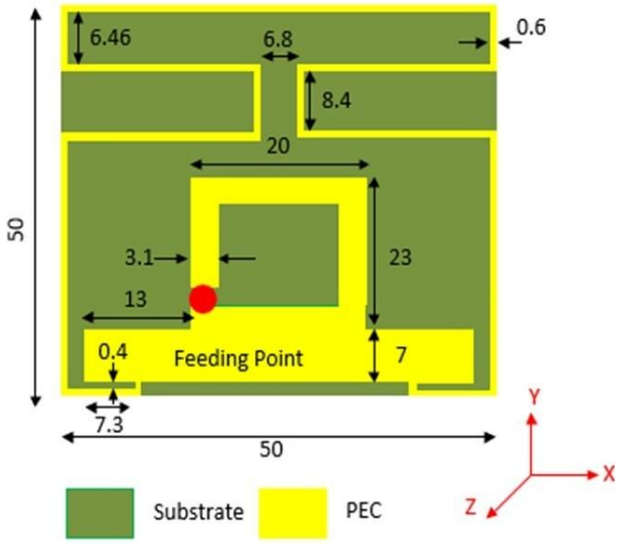

Fig. 6. The proposed antenna at stage 2 (dimensions in mm.)

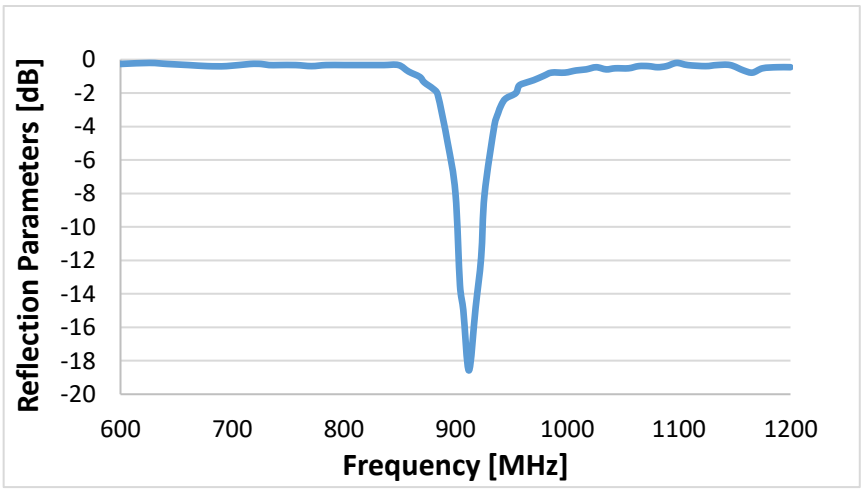

Fig. 7. Reflection coefficient S11 of the proposed antenna in step 3.

Fig. 8 shows the surface current distribution at 915 MHz. It can be clearly seen from the figure that the excited mode is the half wavelength loop mode; this mode is characterized by having a peak current located between two null points in its current distribution. This is also in good agreement with the physical total electrical length of the optimized design. The total length is about 160 mm, which is equivalent to ($\lambda/2$) at 915 MHz.

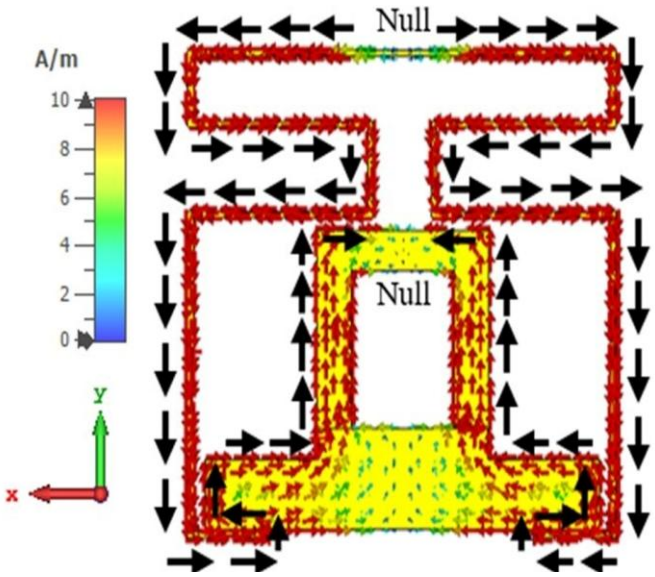

Fig.8. Surface current distribution of the proposed antenna in step 3.

The total radiation efficiency reaches up to 90%, as shown in Fig. 9. The maximum total radiation efficiency is obtained at 915 MHz which is the frequency at which S_{11} is the smallest. This achieved total efficiency ensures capturing a maximum amount of RF energy, leading to the maximization of the overall energy conversion efficiency of the intended integrated rectenna.

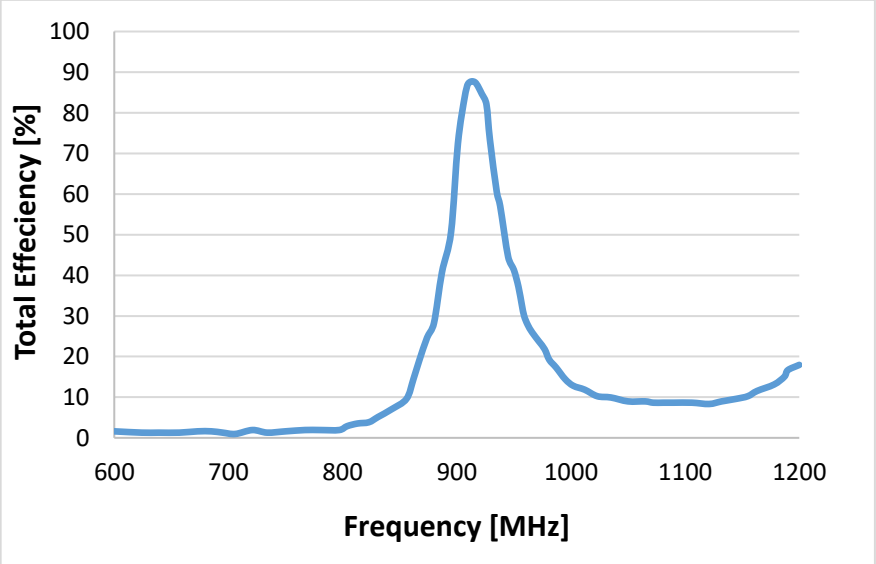

Fig. 9. Total radiation efficiency of the final optimized antenna.

A maximum realized gain of 3.93 dBi has been obtained. This is a good gain value for a half-wavelength loop resonating at 915 MHz. The antenna obtains an omnidirectional radiation pattern in the XZ-plane, which is typical for loop antennas as can be seen in Figs. 10 and 11, respectively.

The radiation pattern has nulls at phi= 90 and -90 degrees in the YZ and XY-planes. This type of radiation pattern is preferred for the purposes of energy harvesting in order for the antenna to pick the signal from different directions.

The good performance of the antenna in terms of -10 dB bandwidth and strong radiation characteristics (radiation efficiency and gain) makes it a good candidate for energy harvesting.

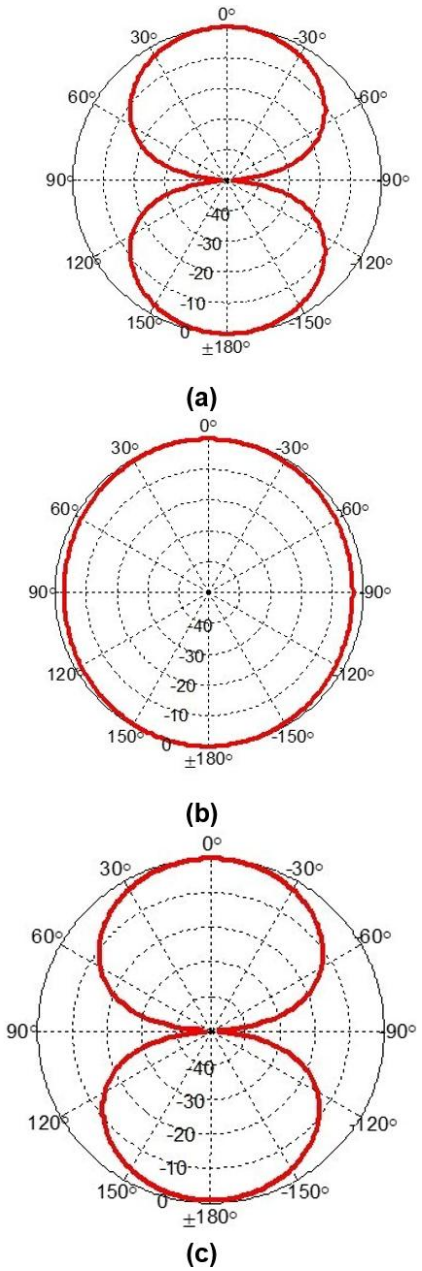

Fig. 10. The 2D (polar plot) radiation patterns of the energy harvesting antenna at the 915 MHz resonance frequency in: a) YZ; b) XZ; c) XY planes.

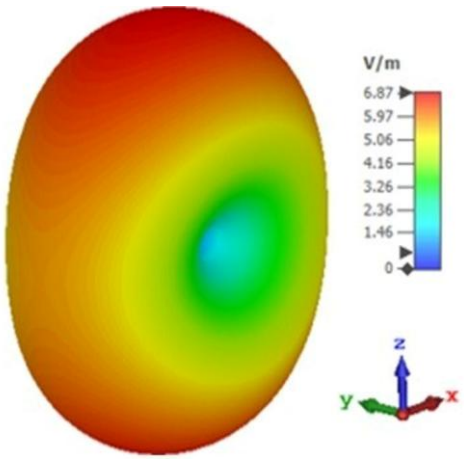

Fig. 11. 3D radiation pattern of the optimized proposed antenna.

2.2. Numerical Validation of the Antenna Design

To validate the performance of the proposed antenna, its design was rigorously modeled using reliable full-wave simulators employing different numerical techniques, specifically the Finite Element Method (FEM) in ANSYS HFSS [42]. Fig. 12(a) and Fig. 12(b) illustrate a strong agreement between the CST Microwave Studio results and the ANSYS HFSS results for the reflection coefficient and total radiation efficiency, respectively. This consistency underscores the reliability of the obtained results using the Finite-Difference Time-Domain (FDTD) method in CST, confirming the robustness of the proposed antenna design. In both figures, the only differences between the results are in the level of matching and the maximum total radiation efficiency. However, the overall antenna bandwidth remains unchanged so that the frequency band under interest is covered.

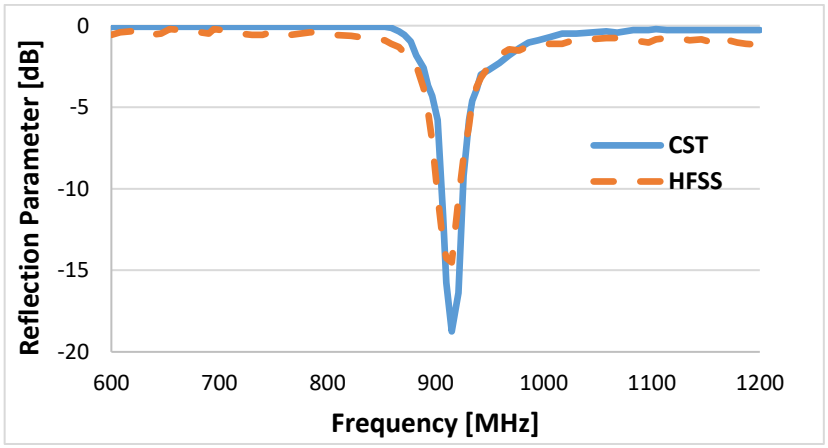

(a)

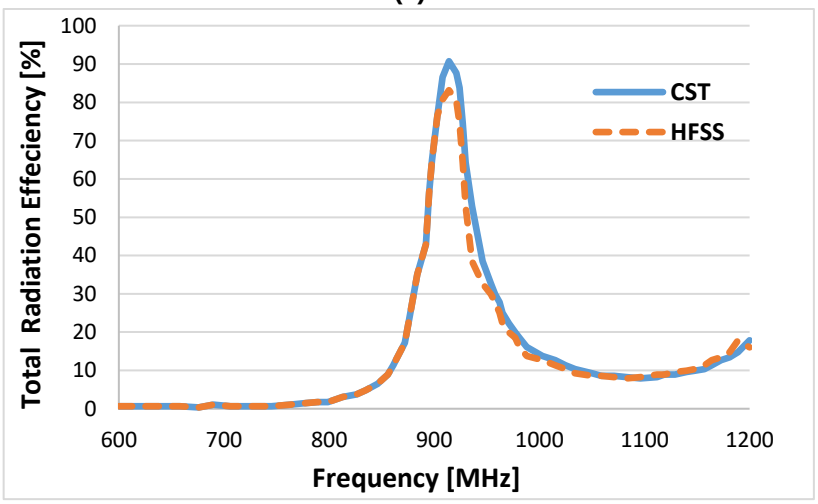

(b)

Fig. 12. Antenna's simulation from CST Microwave Studio and ANSYS HFSS: a) reflection coefficient; b) total radiation efficiency.

2.3. Rectifier Design

The rectifier circuit is an important part of the RF energy harvesting system. It is used to convert the received radio frequency electric current from the antenna to DC current suitable for a specific load. As the proposed antenna is a loop structure, which does not have a common ground. It is worth mentioning that the rectifier circuit can be designed after the feeding coaxial connector, on a separate small PCB board as explained in [43].

A one-stage voltage doubler rectifier topology is utilized, as shown in Fig. 13. This configuration consists of two capacitors and two diodes, arranged as depicted in the figure. The rectifier circuit is based on zero bias Schottky detector diode HSMS 2852 and it is designed using the numerical model in Key Sight Advanced Design System (ADS) [44].

The rectifier receives the RF signals captured by the antenna at 915 MHz at its input and is connected to a load resistance at its output. The load resistance is variable with values ranging between 10 to 100 kΩ.as shown in Fig. 14.

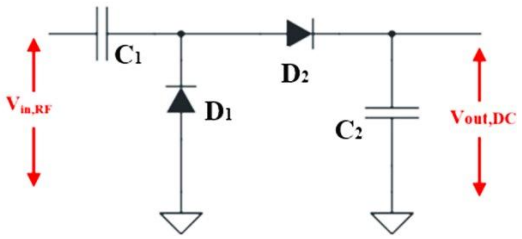

Fig. 13. Schematic diagram of the designed single stage voltage doubler circuit.

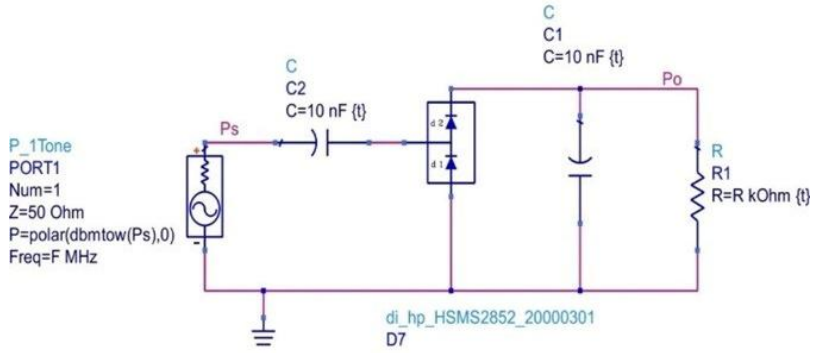

Fig. 14. Schematic diagram of the circuit represented in ADS without matching network.

As mentioned above, zero biased Schottky barrier diode HSMS 285x is used. The modelling parameters of the diode obtained by Software Process Improvement and Capability Determination (SPICE parameters) circuit simulation program [44, 45] are summarized in Table.1.

Table 1. SPICE parameters of the HSMS285X rectifier.

Parameter	Description	Unit	HSMS285X
BV	Reverse breakdown voltage	V	3.8
Cj0	Zero-bias junction capacitance	pF	0.18
EG	Band-gap energy	eV	0.69
IBV	Current at breakdown voltage	A	3×10-4
IS	Saturation current	A	3×10-6
N	Emission coefficient	-	1.06
RS	Ohmic resistance	Ω	25
PB(VJ)	Junction potential	V	0.35
PT(XTI)	Saturation-current temp.exp	-	2
M	Grading coefficient	-	0.5
If	Forward current	A	N/A
PIV	Peak inverse voltage	V	2
TSTG	Storage temperature	◦C	-65 - 150
PD	Device dissipation	mW	75
	Frequency range	-	below 1.5 GHz

The reflection coefficient between the rectifier and antenna is evaluated by simulating the rectifier circuit with an input resistance of 50 Ω approximately. Large reflection losses were introduced for the circuit at this stage as shown in Fig. 15.

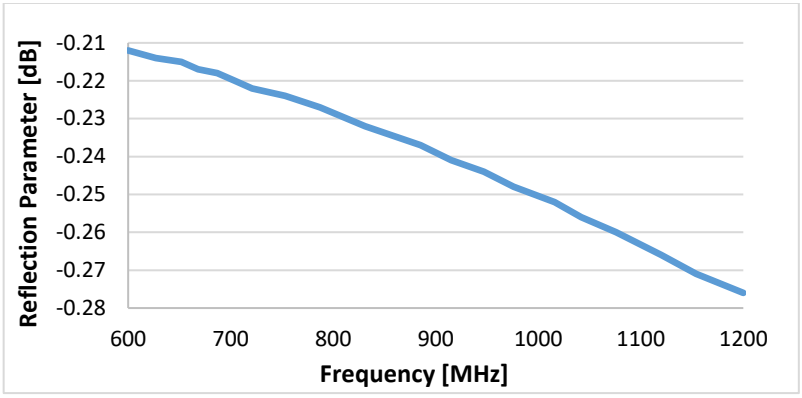

Fig. 15. The reflection coefficient between the antenna and matching circuit before matching.

The reflection coefficient results indicate that ~95% (~ -2.38 dB) of the input power is almost reflected. However, no more than 10% of power reflection should be maintained. The reflection coefficient (S_{11}) should be ≤ -10 dB [46].

$$S_{11} = 10\log_{10}(\frac{P_{ref}}{p_{in}}) \quad (8)$$

where P_{ref} (W) is the reflected power and P_{in} (W) is the input power. Based on the results above, a matching circuit is needed between the antenna and rectifier, which is designed and presented in the following section.

2.4. Matching Circuit Section Design

There are two main types of matching networks that can be used for high frequency circuits: i) lumped-element network which comes in different topologies (L, π or T-sections) or ii) distributed circuit elements like transmission line stubs, in which different sections (quarter wavelength, single series or parallel or double series or parallel stubs) of the transmission lines are used as the matching section. The lumped element network is preferred for sub-GHz applications as its insertion loss is very low. The L-section has been selected specifically because it is simpler than the other π- or T- sections. A simple LC-matching section is used. The values of optimum L and C are derived from the ADS simulator. They are 61.25 nH and 4.64 pF for inductance (L) and capacitance (C), respectively. The overall structure, including the matching section, is illustrated in Fig. 16.

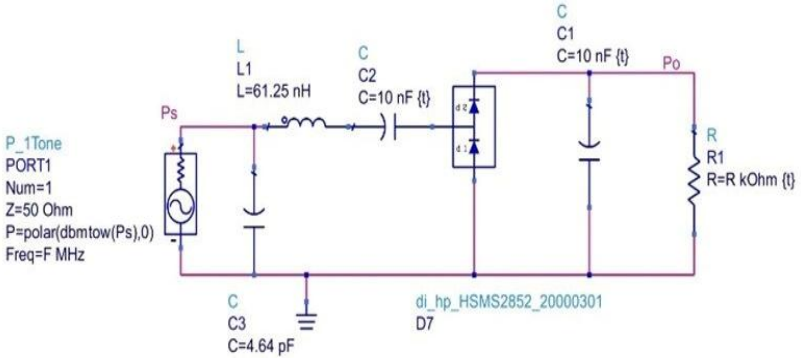

Fig. 16. The matching L-section with the rectifier in ADS.

The total input impedance is now purely resistive, with a value close to 50 Ω (approximately 48.996 Ω). The reflection coefficient after adding the matching section is depicted in Fig. 17. As shown in the figure, the reflection coefficient is well below -10 dB for the intended band, meeting the required specifications.

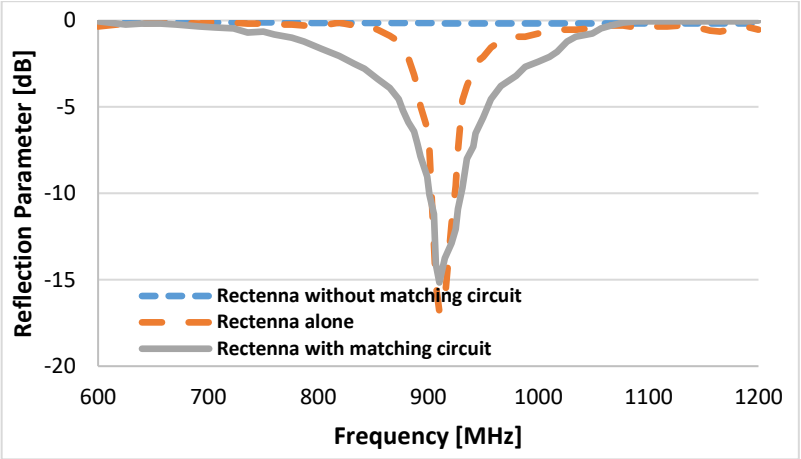

Fig. 17. The reflection coefficient for the antenna without filter and for the antenna with a matched and unmatched filters.

2.5. Numerical Validation of the Rectifier Design

To validate the rectifier results (Rectenna), which are obtained using ADS, we have used CST Design Studio in modeling the linear model of the zero barrier Schottky barrier diode HSMS 2852, which is the same diode that used in ADS, Fig. 18(a) shows the diode model that was used in CST design studio.

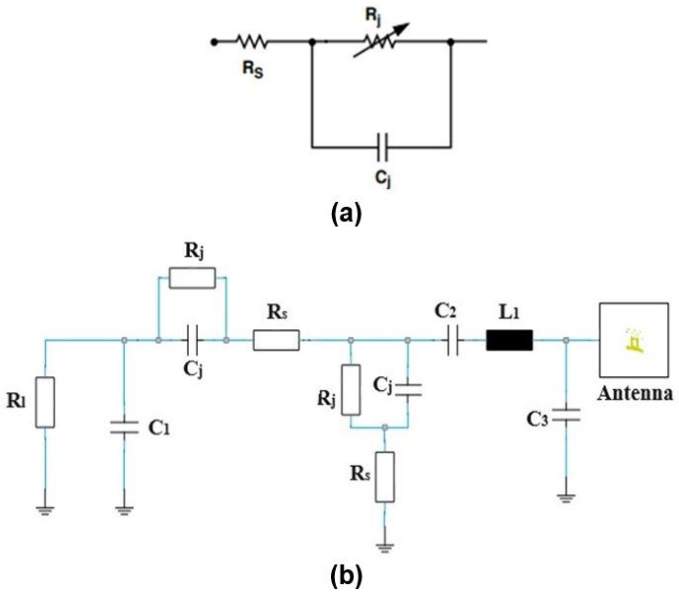

Fig. 18. CST Design Studio results: a) HSMS 2852 Diode Model; b) rectifier circuit with L-section matching circuit.

The used spice model was extracted from the data sheet of diode supplied by diode manufacturer [47], then it is added into components library of CST design studio. Then the optimized antenna in CST Microwave Studio was used as an RF input generator/source in CST Design Studio; this is done by importing the equivalent circuit model of the optimized antenna from the CST Microwave Studio to CST Design Studio.

The complete CST Design Studio circuit model with the designed matching circuit is shown in Fig. 18. It is worth mentioning that R_s represent a series resistance, R_j and C_j are the junction resistance and capacitance, respectively. The results of the reflection coefficient from both the CST Design Studio and the ADS are attached in Fig. 19. It can be seen they have a good agreement over the entire operational bandwidth.

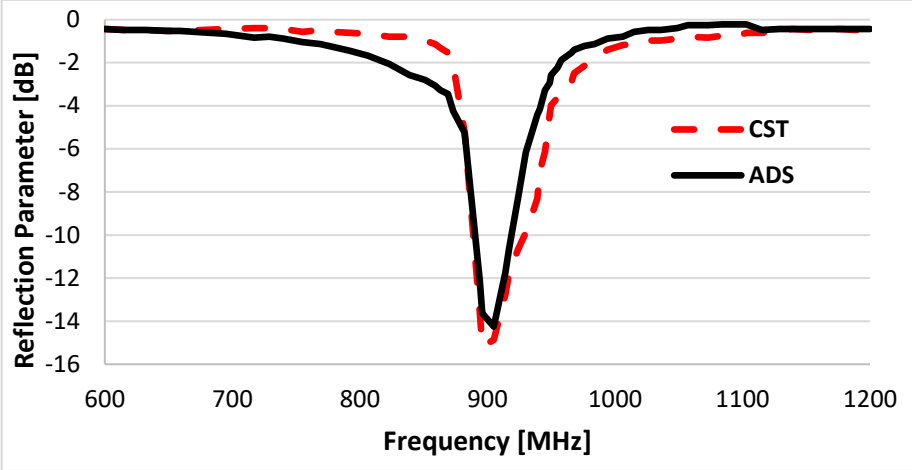

Fig. 19. Reflection coefficient for the rectenna without filter and for the antenna with a match and filter.

3. THE OVERALL RECTENNA PERFORMANCE

One of the main evaluation parameters of the rectenna performance is the conversion efficiency:

$$\eta_{conv} = \frac{P_{DC}}{P_{AC}} \tag{9}$$

where P_{DC} (W) is the DC power delivered to the load, P_{AC} (W) is the AC power input to the rectenna. An effective rectenna system should be able to convert the largest of the AC power received by the antenna to DC power delivered to the load.

The RF to DC conversion efficiency of the RF energy harvesting system is determined by simulating various input RF power levels to the rectifying circuit while varying the resistive load value. This is to select the optimum load resistance value which obtains the highest conversion efficiency with a suitable input power. The power conversion efficiency can be seen in Fig. 20.

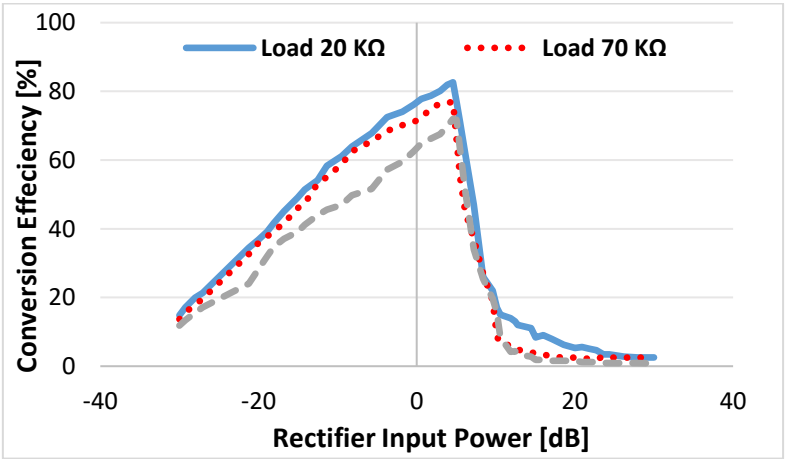

Fig. 20. PCE of the proposed rectenna for different input power levels and variable load resistance in ADS.

The figure indicates that up to 80% was observed at 915 MHz observed with an input power of 5 dBm and load of 20 KΩ. This is a high value of the conversion efficiency. However, an input power of -15 dBm is usually specified for energy harvesting applications [11].

The effect of the load resistance on the power conversion efficiency at this input power level at 915 MHz is shown in Fig. 21. Based on the ADS simulation result, the figure indicates that a maximum efficiency of 53% is obtained at the load resistance of 20 KΩ. Additionally, the figure shows the conversion efficiency result from the CST Design Studio, which has the same pattern. However, it is less that the results obtained from the ADS by 1% to 2%.

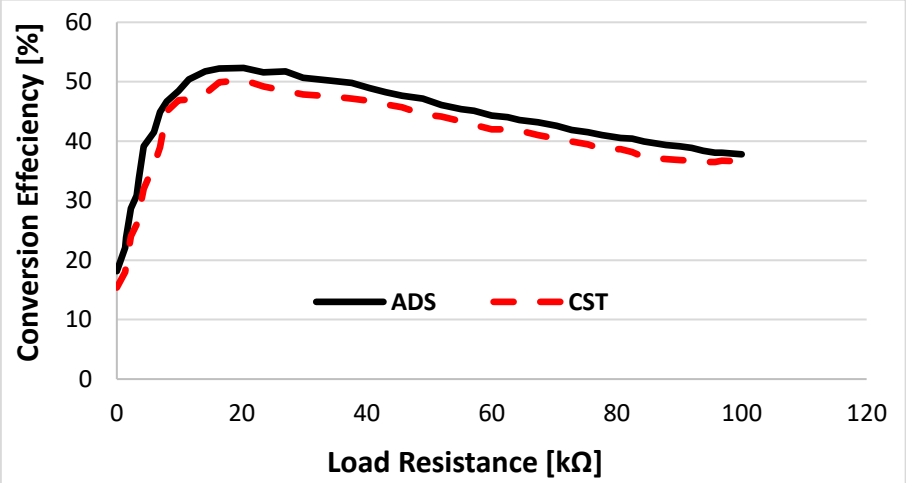

Fig. 21. Power conversion efficiency at 915 MHz and -15 dBm power input.

Additionally, the conversion efficiency as function of the frequency for a consistent power of -15 dBm is computed and presented in Fig. 22.

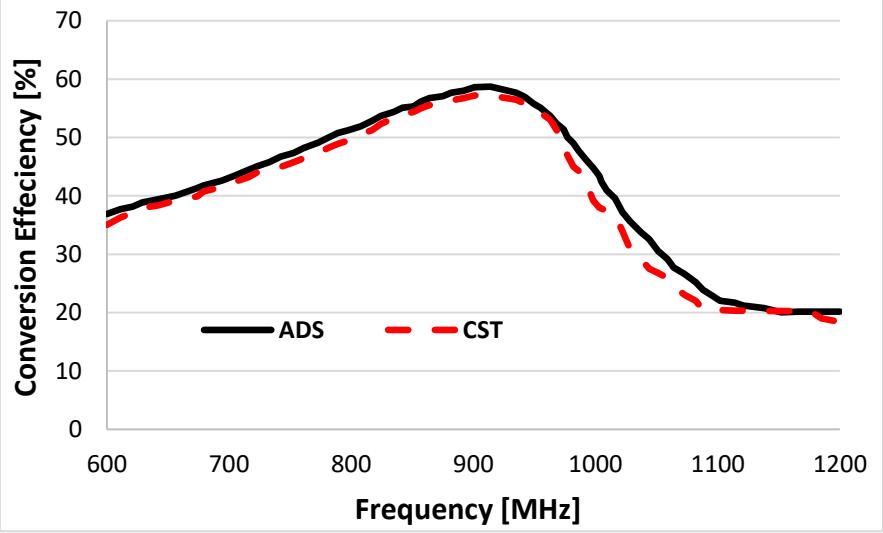

Fig. 22. Power Conversion Efficiency over frequencies at 20 kΩ load.

It can be seen from the figure that the maximum conversion efficiency is obtained at 915 MHz. This is expected as the rectenna obtained the best matching level at this frequency. It can be concluded from the results above that the proposed antenna can be used with a maximum input power of -15 dBm at 915 MHz, obtaining a maximum conversion efficiency of

58%. The main characteristics of the proposed rectenna system are summarized and compared with other relevant works in Table. 2.

Table. 2. Comparison between the proposed and – reported in literature - rectenna systems

Ref.	Frequency [MHz]	Max planar Dimensions [mm]	Type of diode	PCE [%]; Pin [dBm]	Rectifier Topology	Matching circuit topology	Flexibility
[6]	433, 915	100x100	BAT 15	47.2, 33.3; 10	Voltage doubler	Inductive	No
[7]	2450	80x60	SMS7630	70; 0	Single diode	L-section	yes
[8]	2450	N/A	SMS7630	55.7; 8	Single diode	N/A	yes
[9]	465	150x5 (E-field) 77.6x40 (H-field)	HSMS28 2C	76.3; 17.5 88.5; 22.2	Voltage doubler	L-shaped LC network	yes
[10]	900, 1900, 2400	90x40	HSMS 285C	80; 10 46;8 40;16	Four stage voltage multiplier	LC voltage boosting network	No
[11]	900, 1800, 2100	84x35	SMS763 0-079	27.3; -20 20, -20 14, -20	Voltage doubler	Triple stub	No
[12]	915	10.5×6	HSMS2850	42 ; >-15	Single diode	Single stub , inductive	No
[13]	2450	50×50	HSMS 2852	52; 0	Voltage doubler	L-section	No
[14]	1950 2450	50×50	HSMS2850	63; 14 69; 15.5	Voltage doubler	Four section lines	No
[15]	2450	50×11.5	SMS7630	16; -15	Single diode	A dual trans. line	yes
[16]	2450	42.92×42.92	SMS7630	6.2; -15	Single diode	N/A	yes
[17]	915	92×76	HSMS2850, HSMS2860	30; -15	Adaptive with FET	L-section	yes
[18]	900, 1800	20×20	HSMS285x	28, 20; -20	Voltage doubler	N/A	No
[19]	402, 433, 2450	10×10×2.45	HSMS-286c	86; 11 <10; -15	Voltage doubler	N/A	No
[20]	900, 1800, 2100	78×50	HSMS 285B	32.3, 35.5, 18.6; -5	Multi-stage voltage multiplier	Lumped Elements and Trans. Line	No
[21]	900, 1800, 2450 2100	80× 80×0.8	HSMS-2822, HSMS-2852	90, 80, 42; -27.5 48; -35	Multi-stage voltage multiplier	LC matching	yes
[22]	1.7-2.8	55×55×1	HSMS2860	40; -3	Voltage doubler	LC matching	No
[27]	900, 1800, 2100	78×50	HSMS 285B	5, 20, 23, -15	Single diode	Double stub	No
[28]	2450	45x41	HSMS 270B, 5456a	70.58 ; 0	Voltage doubler	L-section	No
[29]	915	7.9 × 7.7	HSMS 2852	45; 5	Voltage doubler	L-section	No
[30]	2450	24.9 × 8.6	HSMS-2852	20; -20	Voltage doubler	L-section	No
[31]	2450	40×40	HSMS 2850	80; -20	Voltage multiplier	LC matching	No
[This work]	915	50×50	HSMS2852	58; -15	Voltage doubler	L-section	yes

The comparison indicates that most of previous designs proposed in literature were rigid [10-13, 20, 22, 27]. The proposed flexible designs were either large in size [9], or worked in the 2.45 GHz ISM band which made them easier to miniaturize [7, 8, 15, 16, 19, 28, 30, 31]. This means that the antenna will have a smaller size. However, this is attributed to the high frequency and not to the antenna structure itself for this case. Although the flexible antenna in [17] operated in the 915 MHz ISM bands, it was 64% larger in size than our proposed antenna. It also had a PCE that was around 48.3% smaller than that of the antenna proposed in this paper. While other designs at 915 MHz such as in [12, 18, 29] had a smaller size, they had a smaller conversion efficiency than that for the design proposed in this paper. Other flexible designs were also proposed in [9] at 465 MHz. However, it obtained a large size. Moreover, it was evaluated for large input power levels of 17.5 and 22.2 dBm and hence it obtained a relatively high PCE of 76.3 and 88.5%, respectively. It is worth noting that the proposed antenna in this paper has achieved a PCE of 80% for an input power of 5 dBm.

While the antenna in [14] has obtained the same size of ours, it is rigid (not flexible) and did not work for the 915 MHz. Moreover, it was evaluated for high input power levels much larger than -15 dBm.

Most of the proposed designs had obtained a much smaller power conversion efficiency not exceeding 33% when compared to the proposed design at an input power of -15 dBm [15-17, 27]. The maximum PCE was also smaller for the surveyed designs in [6, 11, 20, 27] in around the 915 MHz band in comparison with the design proposed in this work. In addition, although the design in [16] was evaluated at the same input power of -15 dBm, it obtained a very small PCE of 6.2% only. This is 89.3% smaller than the PCE obtained for our proposed rectenna. While the design in [21] achieved a radiation efficiency of 90% at around 915 MHz, its size was 60.9% larger than that of the proposed design. Moreover, its rectifier and overall structure were more complicated. On the other hand, the design in [22] achieved a PCE of 40%, which is 31% lower than that of our proposed design.

To sum up, the system proposed in this paper is probably the smallest flexible energy harvesting system at 915 MHz that obtains a conversion efficiency of 58%.

4. CONCLUSIONS AND FUTURE WORK

In this paper, a small, flexible rectenna has been proposed for energy harvesting in the 915 MHz ISM band. It has a small size of 50×50 mm^2 which is about 17% smaller than the smallest flexible rectenna system proposed in literature for this frequency band. In addition to the small size, the proposed energy harvesting system has many appealing features for modern communication systems, such as good radiation characteristics (radiation efficiency, gain, and omnidirectional radiation pattern) and simplicity. Moreover, it is flexible, making it more suitable for different structures as it can be easily attached to them. The overall system has been carefully optimized utilizing a meandered loop structure to obtain miniaturization with high efficiency of 90% and omnidirectional radiation pattern. A single stage voltage doubler rectifier has been selected for the design to boost the input voltage in addition to rectification. To maintain simplicity while reducing power losses between the antenna and rectifier, a matching network based on a simple LC-section was used.

The proposed system obtained a high PCE of up to 80% for loads ranging between 10 and 100 kΩ at a frequency of 915 MHz. The system has obtained a PCE of 58% for an input power of -15 dB, outperforming other energy harvesting system operating at the same frequency.

Additional work can be done in the future, including:

a) Evaluating the bending effect: as the antenna is flexible, it can be bent around different structures, and hence the effect of bending on its performance should be examined. The maximum radius of curvature for which the performance can be maintained might be then determined.
b) Reducing the antenna size: although the proposed antenna is small in size, its size can be further reduced through various techniques and structures, such as split rings. Split rings offer numerous benefits including miniaturizing the antenna and optimizing its matching. Hence, they can be used to match the antenna in the proposed design directly with the filter which results in reducing the design complexity.
c) Enhancing dual-band functionality: the performance can be improved to cover additional bands such as the 2.45 GHz ISM band, by incorporating more than one split ring into the design.

REFERENCES

[1] Q. Awais, Y. Jin, H. Chattha, M. Jamil, H. Qiang, B. Khawaja, ''A compact rectenna system with high conversion efficiency for wireless energy harvesting,'' *IEEE Access*, vol. 6, pp. 35857-35866, 2018, doi: 10.1109/ACCESS.2018.2848907.

[2] K. Dong, Z. Yi, T. Jia, S. Wu, ''2.4 GHz wide band high efficiency rectenna with three sector branches,'' International Conference on Artificial Intelligence, Information Processing and Cloud Computing, 2022, doi: 10.1109/AIIPCC57291.2022.00060.

[3] C. Xu, Y. Fan, X. Liu, ''A circularly polarized implantable rectenna for microwave wireless power transfer,'' *Micromachines,* vol. 13, no. 123, pp. 1-23, 2022, doi: 10.3390/mi13010121.

[4] S. Alja'Afreh, C. Song, Y. Huang, L. Xing, Q. Xu, "A dual-port, dual-polarized and wideband slot rectenna for ambient RF energy harvesting," European Conference on Antennas and Propagation, 2020, doi: 10.23919/EuCAP48036.2020.9135441.

[5] J. Zhu, Z. Hu, C. Song, N. Yi, Z. Yu, Z. Liu, S. Liu, M. Wang, M. Dexheimer, J. Yang, H. Cheng, ''Stretchable wideband dipole antennas and rectennas for RF energy harvesting,'' *Materials Today Physics*, vol. 18, no. c, pp. 1-23, 2021, doi: 10.1016/j.mtphys.2021.100377.

[6] M. Wagih, A. Weddell, S. Beeby, ''Dispenser printed flexible rectenna for dual-ISM band high-efficiency supercapacitor charging,'' IEEE Wireless Power Transfer Conference, 2021, doi: 10.1109/WPTC51349.2021.9458070.

[7] J. Zhang, Y. Wang, ''A flexible wearable rectenna for wireless energy harvesting,'' Asia-Pacific Conference on Antennas and Propagation, 2019, doi: 10.1109/APCAP47827.2019.9472112.

[8] J. Zhang, Y. Wang, R. Song, Z. Kou, D. He, ''Highly flexible graphene-film-based rectenna for wireless energy harvesting,'' *Energy and Environmental Materials*, vol. 7, no. 2, pp. 1-6, 2022, doi: 10.1002/eem2.12548.

[9] J. Bito, J. Hester, M. Tentzeris, ''Ambient RF energy harvesting from a two-way talk radio for flexible wearable wireless sensor devices utilizing inkjet printing technologies,'' *IEEE Transactions on Microwave Theory and Techniques*, vol. 63, no. 12, pp. 4533– 4543, 2015, doi: 10.1109/TMTT.2015.2495289.

[10] B. Pham, A. Pham, ''Triple bands antenna and high efficiency rectifier design for RF energy harvesting at 900, 1900 and 2400 MHz,'' IEEE MTT-S International Microwave Symposium Digest, 2013, doi: 10.1109/MWSYM.2013.6697364.

[11] S. Shen, C. Chiu, R. Murch, ''A dual-port triple-band l-probe microstrip patch rectenna for ambient RF energy harvesting,'' *IEEE Antennas Wireless Propagation Letters,* vol. 16, pp. 3071–3074, 2017, doi: 10.1109/LAWP.2017.2761397.

[12] Q. Xu, Y. Huang, X. Zhu, S. Alja'Afreh, L. Xing, ''A new antenna diversity gain measurement method using a reverberation chamber,'' *IEEE Antennas and Wireless Propagation Letters*, vol. 14, pp. 935-938, 2015, doi: 10.1109/LAWP.2014.2386971.

[13] L. Prashad, H. Mohanta, H. Mohamed, ''A compact circular rectenna for RF-energy harvesting at ISM band,'' *Micromachines,* vol. 14, no. 4, p. 825, 2023, doi: 10.3390/mi14040825.

[14] M. Aboualalaa, H. Elsadek, ''Rectenna systems for RF energy harvesting and wireless power transfer,'' *Recent Wireless Power Transfer Technologies,* 2020, doi: 10.5772/intechopen.89674.

[15] A. Eid, J. Hester, A. Nauroze, T. Lin, J. Costantine, Y. Tawk, ''A flexible compact rectenna for 2.40Hz ISM energy harvesting applications,'' IEEE International Symposium on Antennas and Propagation & USNC/URSI National Radio Science Meeting, 2018, doi: 10.1109/APUSNCURSINRSM.2018.8608525.

[16] M. Borgoñós-García, A. López-Yela, D. Segovia-Vargas, ''Rectenna at 2.45 GHz for wearable applications,'' 14th European Conference on Antennas and Propagation, 2020, doi: 10.23919/EuCAP48036.2020.9135476.

[17] A. Almohaimeed, M. Yagoub, J. Lima, R. Amaya, G. Xiao, Y. Tao, ''Metasurface-based WPT rectenna with extensive input power range in the 900 MHz,'' IEEE Canadian Conference on Electrical & Computer Engineering, 2018, doi: 10.1109/CCECE.2018.8447782 .

[18] J. Tissier, M. Latrach, ''A 900/1800 MHz dual-band high-efficiency rectenna,'' vol. 61, vo. 4, pp. 1278-1283, 2019, doi: 10.1002/mop.31704.

[19] F. Huang, C. Lee, C. Chang, L. Chen, T. Yo, C. Luo, ''Rectenna application of miniaturized implantable antenna design for triple-band biotelemetry communication,'' *IEEE Transactions on Antennas and Propagation,* vol. 59, no. 7, pp. 2646-2653, 2011, doi: 10.1109/TAP.2011.2152317.

[20] O. Assogba, A. Mbodji, A. Bréard, A. Diallo, Y. Duroc, ''Tri-band rectenna dedicated to UHF RFID, GSM-1800 and UMTS-2100 frequency band,'' *Sensors*, vol. 22, no. 9, p. 3565, 2022, doi: 10.3390/s22093565.

[21] P. Kar, M. Islam, ''Design and performance analysis of a rectenna system for charging a mobile phone from ambient EM waves,'' *Heliyon*, vol. 9, no. 3, pp. 1-44, 2023, doi: 10.1016/j.heliyon.2023.e13964.

[22] S. Alja'Afreh, Y. Huang, L. Xing, ''A compact wideband and low profile planar inverted-l antenna, 8th European Conference on Antennas and Propagation, 2014, doi: 10.1109/EuCAP.2014.6902529.

[23] N. Khan, F. Khan, U. Farina, ''RF energy harvesters for wireless sensors, state of the art, future prospects and challenges: a review,'' *Physical and Engineering Sciences in Medicine*, vol. 47, pp. 385–401, 2024, doi: 10.1007/s13246-024-01382-4.

[24] A. Altakhaineh, S. Alja'Afreh, A. Almatarneh, E. Almajali, L. Al-Tarawneh, J. Yousaf, "A quad-band shared-aperture antenna based on dual-mode composite quarter-mode SIW cavity for 5G and 6G with MIMO capability,'' *Electronics*, vol. 12, no. 11, p. 2480, 2023, doi: 10.3390/electronics12112480.

[25] H. Chen, C. Sim, C. Tsai, C. Kuo, ''Compact circularly polarized meandered-loop antenna for UHF-band RFID Tag,'' *IEEE Antennas and Wireless Propagation Letters*, vol. 15, pp. 1602-1605, 2016, doi: 10.1109/LAWP.2016.2518215.

[26] S. Alja'Afreh, ''A comparative study of different feeding schemes on the performance of shorted-loop antenna for wireless applications,'' *International Review on Modelling and Simulations*, vol. 16, no. 3, pp. 178-184, 2023, doi: 10.15866/iremos.v16i3.23440.

[27] O. Assogba, A. Mbodji, A. Bréard, A. Diallo, Y. Duroc, ''Tri-band rectenna dedicated to UHF RFID, GSM-1800 and UMTS-2100 frequency bands,'' *Sensors*, vol. 22, no. 9, p. 3565, 2022, doi: 10.3390/s22093565.

[28] R. Pandey, Rashmi, A Shankhwar, S. Ashutosh, ''Design and analysis of wideband rectenna for IoT applications,'' International Conference on IoT Based Control Networks and Intelligent Systems, 2021, doi: 10.2139/ssrn.3769225.

[29] O. Koohestani, J. Tissier, M. Latrach, ''A miniaturized printed rectenna for wireless RF energy harvesting around 2.45 GHz,'' *AEU - International Journal of Electronics and Communications*, vol. 127, p. 153478, 2020, doi: 10.1016/j.aeue.2020.153478.

[30] M. Koohestani, J. Tissier, M. Latrach, ''A miniaturized printed rectenna for wireless RF energy harvesting around 2.45 GHz,'' *AEU - International Journal of Electronics and Communications*, vol. 127, pp. 1-20, 2020, doi: 10.1016/j.aeue.2020.153478.

[31] W. Ali, H. Subbyal, L. Sun, S. Shamoon, ''Wireless energy harvesting using rectenna integrated with voltage multiplier circuit at 2.4 GHz operating frequency,'' *Journal of Power and Energy Engineering*, vol. 10, no. 3, pp. 22-34, 2022, doi: 10.4236/jpee.2022.103002.

[32] S. Kirtania, A. Elger, M. Hasan, A. Wisniewska, K. Sekhar, T. Karacolak, P. Sekhar, ''Flexible antennas: a review,'' *Micromachines*, vol. 11, no. 9, p. 847, 2020, doi: 10.3390/mi11090847.

[33] R. Alrawashdeh, Y. Huang, M. Kod, A. Sajak, ''A broadband flexible implantable loop antenna with complementary split ring resonators,'' *IEEE Antennas and Wireless Propagation Letters*, vol. 14, pp. 1506-1509, 2015, doi: 10.1109/LAWP.2015.2403952.

[34] R. Alrawashdeh, Y. Huang, P. Cao, ''Flexible meandered loop antenna for implants in MedRadio and ISM bands,'' *IEEE Antennas and Wireless Propagation Letters*, vol. 49, no. 24, pp. 1515-1517, 2013, doi: 10.1049/el.2013.3035.

[35] A. Al-Laymoun, R. Alrawashdeh," A spiral flower shape wearable antenna for smart internet of things applications," *Jordan Journal of Electrical Engineering*, vol. 10, no. 2, pp. 212-228, 2024, doi: 10.5455/jjee.204-1685620635.

[36] *CST-Computer Simulation Technology*, 2023, http://www.CST.com.

[37] M. Cos, F. Heras, ''Polypropylene-based dual-band CPW-fed monopole antenna [antenna applications corner],'' *IEEE Antennas and Propagation Magazine*, vol. 55, no. 3, pp. 264-273, 2013, doi: 10.1109/MAP.2013.6586683.

[38] M. Sadiku, J. Buck, *Elements Of Electromagnetics*, Mcgraw Hill Higher Education, 2012.

[39] W. Hayt, J. Kemmerly, S. Durbin, *Engineering Circuit Analysis*, McGraw-Hill, 2012.

[40] C. Balanis, *Antenna Theory: Analysis and Design*, Wiley, 2016.

[41] O. Elalaouy, M. El Ghzaoui, J. Foshi, "A low profile four-port MIMO array antenna with defected ground structure for 5G IoT applications," *Jordan Journal of Electrical Engineering*, vol. 9, no. 4, pp. 496-508, 2024, doi: 10.5455/jjee.204-1673904693.

[42] *ANSYS, High Frequency Structure Simulator,* 2024, https://www.ansys.com.

[43] C. Song, Y. Huang, J. Zhou, J. Zhang, S. Yuan, P. Carter, "A high-efficiency broadband rectenna for ambient wireless energy harvesting," *IEEE Transactions on Antennas and Propagation*, vol. 63, no. 8, pp. 3486-3495, 2015, doi: 10.1109/TAP.2015.2431719.

[44] *Advanced Design System*, 2018, www.keysight.com.

[45] *Simulation Program with Integrated Circuit Emphasis*, 2024, https://www.analog.com.

[46] Y. Huang, K. Boyle, *Antennas from Theory to Practice*, John Wiley & Sons Ltd, 2008.

[47] *HSMS-285x Series*, 2006, https://www.farnell.com/datasheets/47810.pdf.